Magnetic and structural properties of $Ca(Fe_{1-x}Co_x)_2P_2$ and $Ca(Ni_{1-x}Co_x)_2P_2$

Shuang Jia,[1] Songxue Chi,[2,3] J. W. Lynn,[2] and R. J. Cava[1]
[1]*Department of Chemistry, Princeton University, Princeton, New Jersey 08544, USA*
[2]*NIST Center for Neutron Research, National Institute of Standards and Technology, Gaithersburg, Maryland 20899, USA*
[3]*Department of Materials Science and Engineering, University of Maryland, College Park, Maryland 20742, USA*
(Received 30 April 2010; revised manuscript received 11 June 2010; published 28 June 2010)

We report thermodynamic and crystallographic properties for $Ca(Fe_{1-x}Co_x)_2P_2$ and $Ca(Ni_{1-x}Co_x)_2P_2$ for $0 \leq x \leq 1$ both $ThCr_2Si_2$-type solid solutions. $Ca(Fe_{1-x}Co_x)_2P_2$ display an anomalous, non-Vegard's law *a*-axis variation. A monotonically increasing interlayer P-P bond strength is found on progressing from Fe to Co to Ni in the 3*d* series. Both $CaFe_2P_2$ and $CaNi_2P_2$ evolve from Pauli paramagnetic to antiferromagnetic ($CaCo_2P_2$) with Co doping but the magnetic properties of the solid solutions are distinctly different. $Ca(Ni_{1-x}Co_x)_2P_2$ shows more localized-electron behavior, associated with more complicated magnetic phase transitions.

DOI: 10.1103/PhysRevB.81.214446 PACS number(s): 61.50.Ks, 74.25.Jb, 75.30.−m

I. INTRODUCTION

The correlation between magnetic properties and unconventional superconductivity in iron pnictides with the $ThCr_2Si_2$ crystal structure is of great current interest.[1–3] The influence of detailed crystal-structure characteristics on properties is being actively developed. At various temperatures and pressures, the parent compound $CaFe_2As_2$, for example, displays an uncollapsed tetragonal (ucT) phase, an orthorhombic phase, and a collapsed tetragonal (cT) phase while its magnetic state varies from antiferromagnetic (AFM) to superconducting, and then to nonmagnetic.[4,5] Similar to the pressure effect, hole doping on the Ba site by K,[6] or electron doping on the Fe site by Co and Ni in the parent compound $BaFe_2As_2$ also evolves the electronic ground state from AFM to superconducting. Correlations between bond angles and superconducting (SC) transition temperature (T_c) have been made.[6]

The analogous phosphorous system AT_2P_2 (A=Ca, Sr, and Ba; T=Fe, Co, and Ni), albeit showing no unconventional superconductivity, manifests interesting correlations between magnetic properties and crystal structures. Previous studies have pointed out that this system is actually located at the borderline of an interlayer P-P bonding instability, and therefore changing the size of A^{2+} cations, e.g., from Ba^{2+} and Sr^{2+} to smaller Ca^{2+}, induces a lattice-collapse transition from a ucT phase to a cT phase.[7,8] The lattice collapse is driven by the formation of an interlayer P-P bond. Recent theoretical studies inferred that the forming and breaking of a P-P bond result in a shape change for the TP_4 tetrahedra and a charge redistribution within the T_2P_2 layer.[9] Experimental studies show that the magnetic ground state of the $Sr_{1-x}Ca_xCo_2P_2$ solid solution varies from nearly ferromagnetic (FM) Fermi liquid (FL) to AFM, then to FM-like and finally back to AFM, associated with the structural variation from ucT (x=0) to cT (x=1).[10] Physical property differences between the cT and ucT phases were also reported for different Fermi-surface topologies in $CaFe_2P_2$ and $SrFe_2P_2$,[11,12] and the SC ground states in $SrNi_2P_2$ and $BaNi_2P_2$.[13,14]

In this paper, we focus on the structural and magnetic properties of the $Ca(Fe_{1-x}Co_x)_2P_2$ and $Ca(Ni_{1-x}Co_x)_2P_2$ solid solutions. All three parent compounds, $CaFe_2P_2$, $CaCo_2P_2$, and $CaNi_2P_2$ show a cT structure with different P-P interlayer bond lengths from 2.7 Å ($CaFe_2P_2$) to 2.3 Å ($CaNi_2P_2$).[7] $CaCo_2P_2$ displays *A*-type AFM ordering below 90 K in which the cobalt moments are ordered ferromagnetically within the basal *ab* plane but antiferromagnetically along the *c* axis.[8,10,15,16] Both $CaFe_2P_2$ and $CaNi_2P_2$ are normal Pauli paramagnetic metals with no magnetic or SC states down to 2 K.[16] Band-structure calculations have revealed that $CaNi_2P_2$ presents stronger P-P bond strength than $CaFe_2P_2$.[17,18] Those studies also argue that $CaNi_2P_2$ shows a narrow, filled antibonding transition metal—transition metal (T-T) band while in $CaFe_2P_2$ this band is empty.[17] The magnetic character of $CaCo_2P_2$, therefore, is argued to be due to the 3*d* electron correlations when this band is near the Fermi surface (E_F).

The purpose of the current study is to investigate the variation in the crystal structure and magnetic properties associated with the 3*d* electron filling in these compounds, and thereupon understand the correlation between the interlayer P-P bonding and the 3*d* electron configurations. Employing x-ray diffraction (XRD) measurements, we find a non-Vegard's-law behavior of the *a* axis in $Ca(Fe_{1-x}Co_x)_2P_2$, which was not anticipated by the band-structure calculations. Thermodynamic and electron-transport measurements reveal that both Fe and Ni doping-induced magnetic-property variation of $CaCo_2P_2$ can be considered as resulting primarily from band effects but simple *d*-orbital filling in a rigid-band fashion does not explain the observations. Also, the evolution from Pauli paramagnetic metals ($CaFe_2P_2$ and $CaNi_2P_2$) to an *A*-type AFM metal ($CaCo_2P_2$) by means of Co doping, occurs in different ways: $Ca(Ni_{1-x}Co_x)_2P_2$ displays more localized-electron behaviors and more complicated magnetic-phase transitions. These magnetic variations and differences can be understood through bond-length and band-structure changes.

II. EXPERIMENTAL METHODS

Polycrystalline samples were prepared from elemental P (red, 99%), Ca (99.5%), Fe (99.5%), Co (99.8%), and Ni (99%) powder. As the first step, FeP, CoP, and Ni_5P_4 were synthesized as previously described.[19] Then $CaFe_2P_2$ and

 ©2010 The American Physical Society

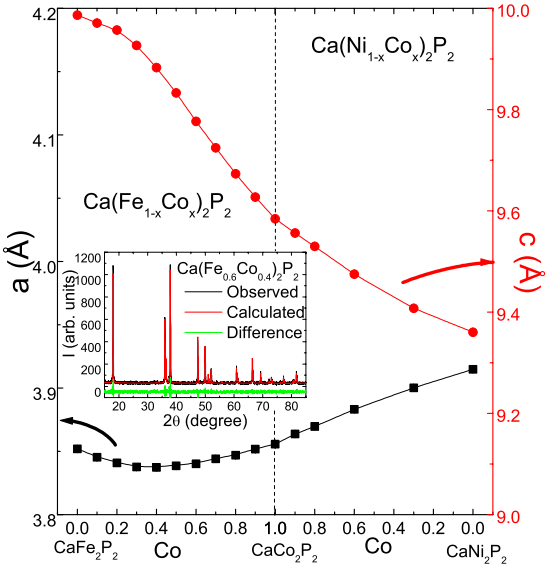

FIG. 1. (Color online) Room-temperature lattice parameters for $Ca(Fe_{1-x}Ni_x)_2P_2$ and $Ca(Ni_{1-x}Co_x)_2P_2$. Inset: XRD pattern and refinement for $Ca(Fe_{0.6}Co_{0.4})_2P_2$.

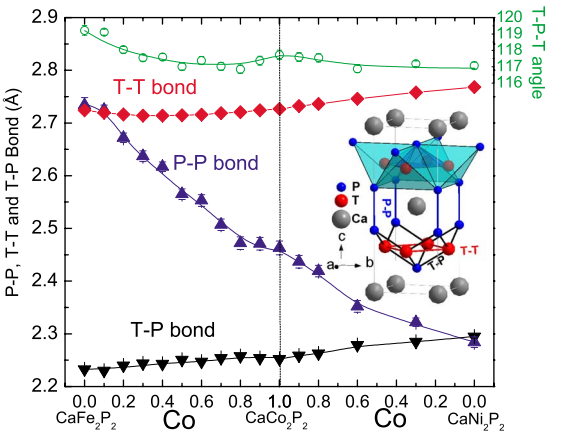

FIG. 2. (Color online) Interlayer P-P bond length and intralayer T-P and T-T (T=Fe, Co, and Ni) bond lengths for $Ca(Fe_{1-x}Co_x)_2P_2$ and $Ca(Ni_{1-x}Co_x)_2P_2$. All the lines are guides to the eyes. Inset: the structure of CaT_2P_2 unit cell.

$CaCo_2P_2$ were made by mixing powder of Ca, FeP(CoP), and P at the ratio of 1.1 Ca: 2 FeP (CoP): 0.1 P. $CaNi_2P_2$ was made from a mixture of the powder of Ca, Ni_5P_4 and P at the ratio of (1.1Ca: $0.4Ni_5P_4$:0.5P). The mixtures were placed in alumina crucibles and sealed in evacuated silica tubes and then heated up to 900 °C for 1 h. In the last step, the results were ground and mixed as $Ca(Fe_{1-x}Co_x)_2P_2$ and $Ca(Ni_{1-x}Co_x)_2P_2$ for $0 \leq x \leq 1$, heated at 1000 °C for 12 h; then the sintered pellets were reground and subsequently pressed into pellets, which were sintered at 1100 °C for 40 h. All the samples were characterized by laboratory x-ray diffraction with Cu $K\alpha$ radiation (D8 Focus, Bruker) at room temperature. Structure analysis was performed by using the program GSAS with EXPGUI.[20,21] All physical property characterization was performed on a Quantum Design Physical Property Measurement System. The neutron-scattering experiments were performed on the triple-axis spectrometers BT7 with a closed cycle ^{4}He cryostat at NIST Center for Neutron Research. Pyrolytic-graphite crystals were used to monochromate and analyze the incident and scattered beams using the 002 reflection, respectively.

III. RESULTS

A. Structural variation

Figure 1 shows the room-temperature lattice parameters ($I4/mmm$, No.139) for $Ca(Fe_{1-x}Co_x)_2P_2$ and $Ca(Ni_{1-x}Co_x)_2P_2$ as a function of Co concentration. While the c axis, a measure of the unit cell perpendicular to the T_2X_2 layers decreases monotonically from T=Fe to Co and then to Ni, the a axis, a measure of the T_2X_2 in-plane dimensions, changes in a non-Vegard's-law manner and shows a minimum value at $Ca(Fe_{0.6}Co_{0.4})_2P_2$. Given that the Goldschmidt radii of Fe, Co, and Ni atoms decrease only slightly with electron count,[22] this non-Vegard's-law behavior clearly reflects an unusual underlying change in electronic structure in the T_2X_2 layers (*vide infra* for detailed discussion). The a axis only varies ~2% for the whole series, less than the relative change in radii and much less than the 6% variation in the c axis.

The origin of the difference between the variation in the interlayer and intralayer dimensions is seen clearly in the variation of the P-P, T-T, and T-P (T=Fe, Co, and Ni) bond lengths (Fig. 2). While the interlayer P-P bond length monotonically decreases by ~20% from 2.74(1) Å for $CaFe_2P_2$ to 2.28(1) Å for $CaNi_2P_2$, the intralayer T-T bond length ($=a/\sqrt{2}$) and T-P bond length vary only ~2–3 %. Thus the primary effect of changing the electron count by $2e$ per transition metal, on going from Fe to Ni, is to change the strength of the P-P bond. The shape and dimension of the TP_4 tetrahedra change very little across the two series whereas the distance between the T_2P_2 layers drops significantly with increasing d electron count due to the increasing strength of the P-P bond.

B. Magnetic properties of $Ca(Fe_{1-x}Co_x)_2P_2$

Figures 3 and 4 present temperature and field-dependent magnetizations for the $Ca(Fe_{1-x}Co_x)_2P_2$ series, respectively. Iron doping suppresses the magnetization of $CaCo_2P_2$ dramatically: only when $x \geq 0.95$, does $M(T)$ show a weak anomaly at T_N, consistent with on-site A-type AFM ordering. This AFM order is then suppressed for Fe concentrations larger than 10%. Small, temperature-independent Pauli paramagnetism is seen for Fe concentrations higher than 50%. This change in properties may be correlated with the anomaly in the a-lattice parameter change at $x \sim 0.4$. The inset of Fig. 3 shows that the high-temperature magnetization of $Ca(Fe_{1-x}Co_x)_2P_2$ displays Curie-Weiss (C-W) behavior with negligible temperature-independent part (χ_0) for $x \geq 0.7$. The parallel character of the $1/\chi$ data sets reflects an invariant value of effective moment per transition-metal atom (μ_{eff}/TM, $TM=Fe_{1-x}Co_x$), and a monotonically decreasing value of Curie-Weiss temperature (θ_{CW}) with Fe

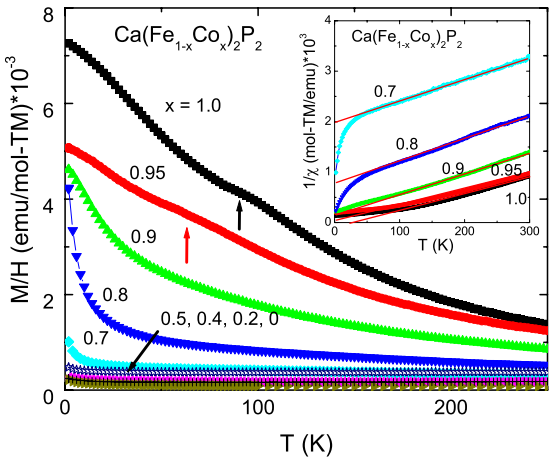

FIG. 3. (Color online) Temperature-dependent M/H for representative members of the $Ca(Fe_{1-x}Co_x)_2P_2$ solid solution in $\mu_0 H = 1$ T. The two arrows indicate the AFM transitions for $x=1$ and 0.95. Inset: high-temperature Curie-Weiss behavior for $x \geq 0.7$. The red lines show the C-W fit.

doping (see Fig. 12). All these features indicate that the electrons associated with the Co and Fe atoms cannot be viewed as simple, local-moment-bearing magnetic impurities in the $Ca(Fe_{1-x}Co_x)_2P_2$ solid solution. The magnetic-property variation associated with Fe doping in this series must be dependent on electron-structure changes near E_F, primarily arising from the decreasing strength of the P-P bond with increasing x.

Figure 5 shows the low-temperature specific-heat data for selected members of the $Ca(Fe_{1-x}Co_x)_2P_2$ series. For $x \leq 0.7$, the data sets show FL behavior ($C_p = \gamma_0 T + \beta T^3$). The γ_0 value increases with x, from ~ 5 mJ/mol K^2 for $x=0$ to ~ 12 mJ/mol K^2 for $x=0.7$. For $x=0.9$, the C_p/T data deviate from FL behavior below 10 K, start to increase below 7 K, and lead to $C_p/T = 25$ mJ/mol K^2 at 2 K. The magnetization data indicate that the system is approaching a magnetic instability when $x=0.9$ (Figs. 3 and 4). Therefore the deviation from FL behavior and large C_p/T at 2 K must be due to magnetic fluctuations near this critical point. When $x=1$, the C_p/T data again show FL behavior with $\gamma_0 = 15$ mJ/mol K^2, although $CaCo_2P_2$ has an AFM ground state. This smaller

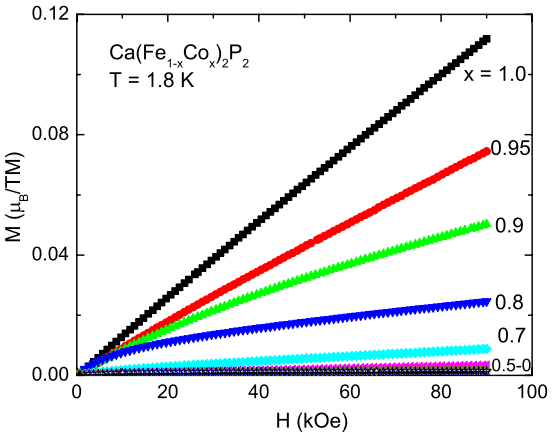

FIG. 4. (Color online) $M(H)$ at 1.8 K for $Ca(Fe_{1-x}Co_x)_2P_2$.

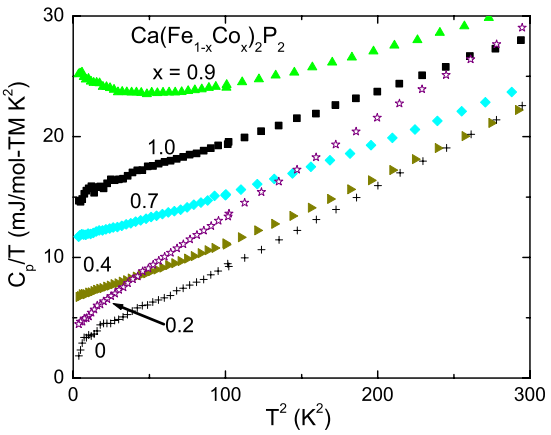

FIG. 5. (Color online) Low-temperature specific heat for the selected members of $Ca(Fe_{1-x}Co_x)_2P_2$ in $H=0$ (plotted as C_p/T vs T^2).

value of γ_0 at $x=1$ indicates that magnetic fluctuations of the conduction electrons have been suppressed by the AFM ordering.

C. Magnetic properties of $Ca(Ni_{1-x}Co_x)_2P_2$

The magnetic properties of $Ca(Ni_{1-x}Co_x)_2P_2$ are significantly different from $Ca(Fe_{1-x}Co_x)_2P_2$ (Figs. 6 and 7). When Ni is doped into $CaCo_2P_2$, the AFM transition shows a more pronounced feature in the temperature-dependent magnetic susceptibility than is seen for $CaCo_2P_2$ (Fig. 6). The magnetic signal below T_N is also significantly suppressed for $x \geq 0.7$. When $x=0.65$ while a high applied field ($\mu_0 H = 1$ T) suppresses the magnetic-ordering feature, the magnetization measured in low field ($\mu_0 H = 0.1$ T) shows a sharp feature at 10 K in a zero-field-cooled (ZFC) warming measurement (inset of Fig. 6). The field-cooled (FC) cooling measurement shows slightly larger signals than the ZFC warming measurement below 10 K but both sets of data are not typical of spin-glass behavior associated with spin freezing.[23] We con-

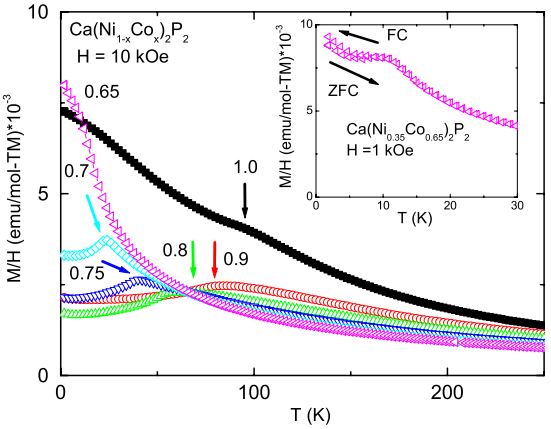

FIG. 6. (Color online) Temperature-dependent M/H for $Ca(Ni_{1-x}Co_x)_2P_2$ solid solution ($0.7 \leq x \leq 1.0$) in $\mu_0 H = 1$ T. The arrows indicate the AFM transitions. Inset: low temperature, ZFC warming and FC cooling M/H for $Ca(Ni_{0.35}Co_{0.65})_2P_2$ in $\mu_0 H = 0.1$ T.

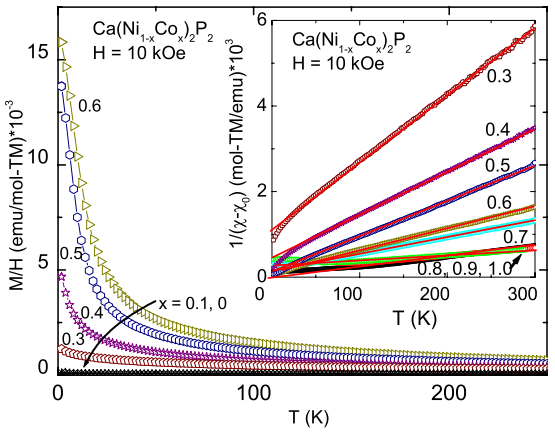

FIG. 7. (Color online) Temperature-dependent M/H for $Ca(Ni_{1-x}Co_x)_2P_2$ solid solution ($0 \leq x \leq 0.6$) in $\mu_0 H = 1$ T. Inset: high-temperature C-W behavior for $x \geq 0.3$. The red lines show the C-W fit.

clude that the magnetic transition in $Ca(Ni_{0.35}Co_{0.65})_2P_2$ at 10 K is more like an AFM ordering associated with some spin frustration. For $0.3 \leq x < 0.65$, the M/H data lose the AFM ordering feature and start to show C-W behavior down to low temperature (Fig. 7). For $x \leq 0.1$, the M/H data become small and temperature independent, reflecting a Pauli paramagnetic state (Fig. 7).

The $M(H)$ curves at 1.8 K for $x \geq 0.7$ are clearly of the AFM type (Fig. 8). The $M(H)$ curves show a faint slope change at various H for $0.7 \leq x \leq 0.9$ (pointed by the arrows in Fig. 8), most likely due to spin reorientation driven by the applied field. The $M(H)$ curve for $Ca(Ni_{0.35}Co_{0.65})_2P_2$ is only linear for $\mu_0 H < 2$ T, which indicates that the magnetic coupling is weak and easily suppressed by the applied field. For $x \leq 0.6$, the $M(H)$ curves are more like Brillouin function, as associated with free, noninteracting local moments. For x

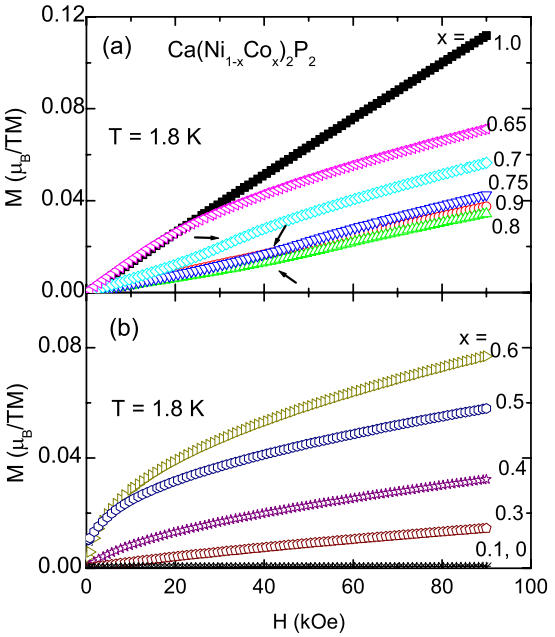

FIG. 8. (Color online) $M(H)$ at 1.8 K for $Ca(Ni_{1-x}Co_x)_2P_2$.

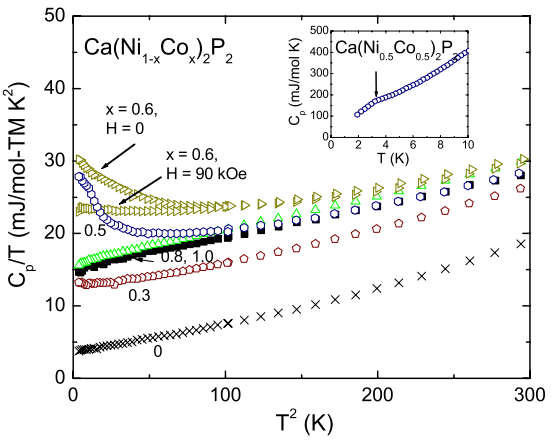

FIG. 9. (Color online) Low-temperature specific heat (plotted as C_p/T vs T^2) for the selected members of $Ca(Ni_{1-x}Co_x)_2P_2$ in $H=0$. The data for $x=0.6$ were measured in $\mu_0 H=0$ and 9 T (pointed by the arrows). Inset: C_p vs T for $x=0.5$ (the arrow shows the anomaly).

$=0.5$, the magnetization data show a small spontaneous magnetization signal, which may indicate the presence of a very small, FM component. This FM-like behavior for $Ca(Ni_{0.5}Co_{0.5})_2P_2$ is consistent with its specific-heat data, which show a faint feature at 3.4 K (inset of Fig. 9). This faint feature may indicate a weak magnetic ordering. Given that the $x=0.6$ sample shows no sign of magnetic ordering in the susceptibility data (see Figs. 7 and 8), the reentrance of a magnetically ordered state for $x=0.5$ is unexpected and should be studied in the future.

The low-temperature specific heat for $Ca(Ni_{1-x}Co_x)_2P_2$ shows FL behavior for $x \leq 0.3$ with γ_0 values increasing with Co concentration (Fig. 9). For $x=0.5$, C_p/T shows a faint feature at 3.4 K unlike the typical λ-like feature associated with a second-order phase transition. The C_p/T data show a clear upturn with decreasing temperature for $x=0.5$ and 0.6. These upturn features are most likely contributed from magnetic fluctuations, which can be suppressed by the applied field, as shown for $x=0.6$ at 9 T. The low temperature C_p/T for $x \geq 0.8$ shows similar FL behavior with $\gamma_0 = 15$ mJ/mol K^2 in the AFM state.

Figure 10 shows the temperature-dependent resistivity (normalized by the resistivity at 300 K) for $Ca(Ni_{1-x}Co_x)_2P_2$. The values of $\rho_{2\ K}/\rho_{300\ K}$ increase with Ni concentration, leading to a maximum value ($\rho_{2\ K}/\rho_{300\ K} \sim 0.9$) at $x=0.65$; they then decrease down to a minimum value ($\rho_{2\ K}/\rho_{300\ K} \sim 0.1$) at $x=0$. For $x \geq 0.65$, the resistivity data show clear slope-change behavior at the magnetic-ordering temperature. This behavior is most likely due to the loss of spin-disorder scattering that occurs with magnetic ordering. The resistivity curves show a slight increase with decreasing temperature for $0.3 \leq x \leq 0.65$, which is reminiscent of the behavior of C_p/T at low temperature. This upturn behavior cannot be explained by the effect of simple, lattice-disorder scattering but must be due to the magnetic scattering of conduction electrons arising with decreasing temperature.

As noted, the temperature-dependent magnetization for Ni-doped $CaCo_2P_2$ shows more pronounced AFM ordering features than $CaCo_2P_2$. The θ_{CW} values drop dramatically on

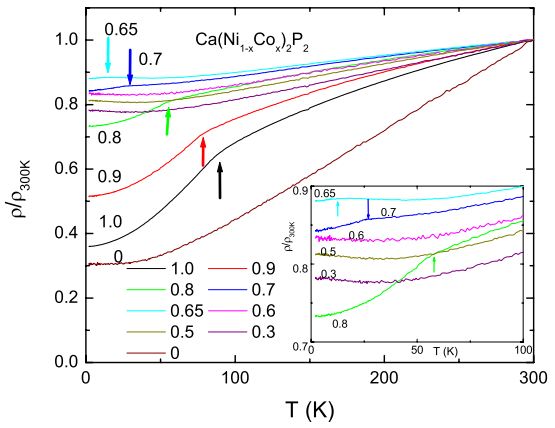

FIG. 10. (Color online) Resistivity for $Ca(Ni_{1-x}Co_x)_2P_2$ (normalized by $\rho_{300\ K}$). Inset: low-temperature part. The arrows show the points of slope change corresponding to T_N.

Ni doping, from 20 K ($x=1$) to −160 K ($x=0.8$) (see Fig. 12). This large, negative θ_{CW} indicates stronger AFM coupling of magnetic moments than is seen for the A-type AFM coupling in $CaCo_2P_2$. The magnetization data suggest that the magnetic ground state may be different for lightly Ni-doped $CaCo_2P_2$. In order to explore the possible magnetic-structure change in this series, neutron-powder diffraction was performed on $Ca(Ni_{0.2}Co_{0.8})_2P_2$ at a low temperature (6 K) and a temperature (80 K) above its T_N (65 K). Figures 11(a) and 11(b) show the low-angle diffraction patterns at 6 and 80 K, and the difference between the data at these two temperatures, respectively. While both data sets show clear diffraction peaks corresponding to the nuclear-structure diffraction, the difference shows no additional diffraction peaks arising from long-range magnetic ordering. The (001) peak arising from the A-type AFM superstructure for the parent compound $CaCo_2P_2$ has been observed previously via powder neutron scattering under similar conditions.[8] Therefore,

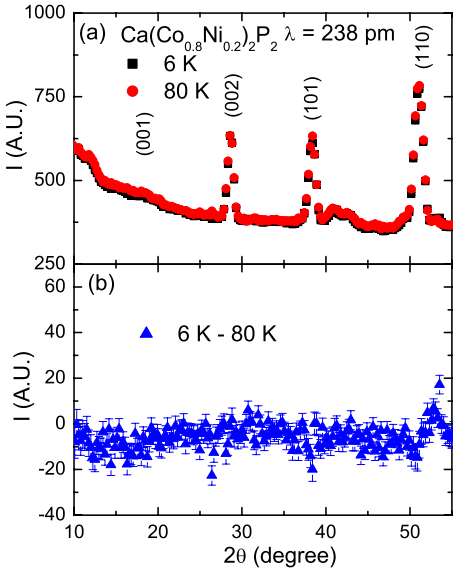

FIG. 11. (Color online) (a) Neutron-scattering measurements for $Ca(Ni_{0.2}Co_{0.8})_2P_2$ at 6 and 80 K; and (b) the difference between the two measurements.

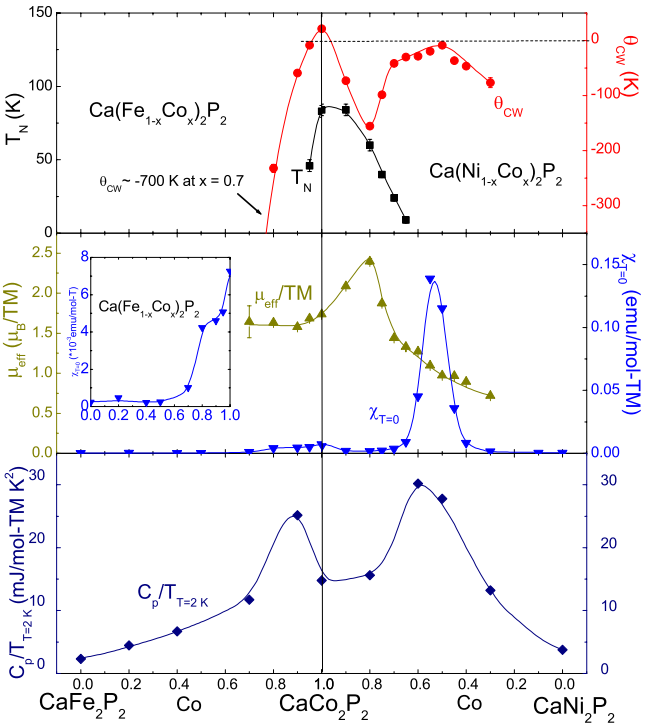

FIG. 12. (Color online) Summary of physical properties for the $Ca(Fe_{1-x}Co_x)_2P_2$ (left) and $Ca(Ni_{1-x}Co_x)_2P_2$ (right) series (all lines are guides to the eye). Upper: T_N and θ_{CW}; middle: effective moment (μ_{eff} per transition metal), zero-temperature susceptibility ($\chi_{T=0} \sim M/H$ at 1.8 K); and lower: C_p/T at 2 K. Inset in the middle panel: $\chi_{T=0}$ for $Ca(Fe_{1-x}Co_x)_2P_2$ with the unit of emu/mol-T*10^{-3}.

our negative result may indicate the disappearance of A-type AFM ordering with Ni doping. Further measurements are needed to determinate the nature of the magnetism present in the Ni-doped materials.

IV. DISCUSSION AND CONCLUSION

The physical properties of $Ca(Fe_{1-x}Co_x)_2P_2$ and $Ca(Ni_{1-x}Co_x)_2P_2$ are summarized in Fig. 12. Both series show high-temperature C-W behavior with less than 30% Fe doping and 70% Ni doping. Both T_N and θ_{CW} of $CaCo_2P_2$ are suppressed monotonically with doping but the effect is more pronounced with Fe as opposed to Ni doping. The effective moment (per transition metal) remains a constant with Fe doping. The large, negative θ_{CW} of −700 K in $Ca(Fe_{0.3}Co_{0.7})_2P_2$ (not shown in the plot) may indicate weak, itinerant-magnetic behavior near this region. θ_{CW} and μ_{eff} display more complicated variation with Ni doping. θ_{CW} first decreases to a minimum value ~−160 K at 20% Ni and then increases to a local maximum value close to 0 K at 50% Ni before finally decreasing. μ_{eff} shows a maximum value of ~2.3 μ_B/TM for 20% Ni that corresponds to a minimum point for θ_{CW}. The variation in μ_{eff} with Ni doping indicates that the magnetic property changes within this series are most likely associated with anomalous band-structure changes, rather than with simple, local-moment bearing physics associated with localized magnetic-impurity doping (Fig. 13).

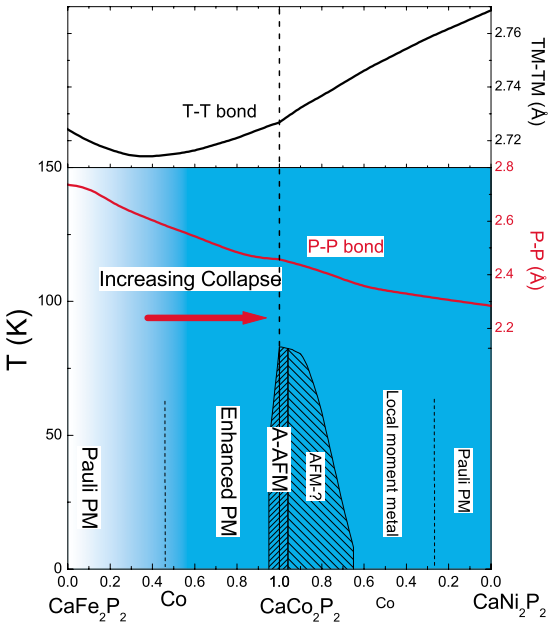

FIG. 13. (Color online) The structural and magnetic phase diagram for $Ca(Fe_{1-x}Co_x)_2P_2$ and $Ca(Ni_{1-x}Co_x)_2P_2$. *A*-AFM: *A*-type antiferromagnetic, AFM-?: antiferromagnetic with unknown structure.

The values of $C_p/T_{T=2\ \mathrm{K}}$ ($=\gamma_0$ for FL state) show two maxima for $Ca(Fe_{0.1}Co_{0.9})_2P_2$ and $Ca(Ni_{0.4}Co_{0.6})_2P_2$. Both maxima occur at the borderline of magnetic instability. The large values of $C_P/T_{T=2\ \mathrm{K}}$ are due to magnetic fluctuations arising from electron correlations. The zero-temperature susceptibility ($\chi_{T=0}$) starts to increase with Co concentration at $x=0.5$ for $Ca(Fe_{1-x}Co_x)_2P_2$ and reaches a maximum value when $x=1$ (inset of Fig. 12). The $\chi_{T=0}$ values for $Ca(Ni_{1-x}Co_x)_2P_2$ are 10^2 times larger than for $Ca(Fe_{1-x}Co_x)_2P_2$ and show a clear maximum for $x\sim0.5$. This maximum corresponds to a FM coupling of the magnetic moments. The variation of $C_P/T_{T=2\ \mathrm{K}}$ is consistent with that of $\chi_{T=0}$, which indicates that both values reflect an underlying evolution of electronic correlations for the whole system.

Previous studies show that the stability of the P-P bond, which determines whether or not the cT or ucT phase forms, is correlated with the number of electrons that are contributed by the transition metal.[7] As shown in Fig. 1, the P-P bond length is significantly larger ($\sim$20%) for $CaFe_2P_2$ than for $CaNi_2P_2$, which indicates that $CaNi_2P_2$ is actually more "collapsed" than $CaFe_2P_2$. This different structure of the cT phases of CaT_2P_2 can be observed in the lattice-collapse transition for T=Fe, Co, and Ni as well. Our previous studies showed that the variation in the lattice parameters for the $Sr_{1-x}Ca_xCo_2P_2$ family is actually more dramatic than for $Sr_{1-x}Ca_xFe_2P_2$, even though both series are believed to pass through a lattice collapse transition upon increased Ca doping. For ANi_2P_2 compounds the lattice collapse transition is always first order and the P-P interlayer distances do not show any intermediate values between the nonbonding and bonding state.[13,24]

Theoretical studies show that the interaction of the P-P orbitals and the *d* orbitals of the transition metals results in an electron-filling change in the P-derived orbitals.[7,9,17,18,25] One argument is that when E_F sinks from the Mn side to the Cu side of the 3*d* metal series, the depopulation of P-P dimer antibonding band leads to increase P-P bond strength.[7] Others argue that increasing the *d*-electron count leads to the filling of the P-P bonding band and the antibonding *T*-P and *T*-*T* bands.[9] The intralayer *T*-*T* and *T*-P bonds are therefore weakened by *d*-electron filling, which leads to a larger intralayer dimension and shorter interlayer distances for simple geometric reasons.[9] Two different effects of the *d*-electron filling have therefore been proposed for making the P-P bond shorter: one is an electronic effect due to the population and depopulation of the P-P dimer bonding and antibonding band, and the other is a geometric effect due to the weakening of the *T*-*T* and *T*-P bonds.

The variation in the lattice parameters and bond lengths of the $Ca(Fe_{1-x}Co_x)_2P_2$ and $Ca(Ni_{1-x}Co_x)_2P_2$ series provides information about the correlation between the *d*-band filling and P-P bonding. In both series, the P-P bond length decreases monotonically, and the *T*-P bond length increases monotonically with increased electron doping, consistent with the calculation results.[9] The minimum *T*-*T* bond length at $Ca(Fe_{0.6}Co_{0.4})_2P_2$, which was not predicted by any theoretical studies, indicates that a simple-geometric effect cannot be the primary reason for the P-P bond variation, at least for the $Ca(Fe_{1-x}Co_x)_2P_2$ series. The P-P bond length at this minimum point is 2.6 Å, which is same as the P-P bond length in the $Sr_{1-x}Ca_xCo_2P_2$ system for $x=0.9$. In the $Sr_{1-x}Ca_xCo_2P_2$ series, $x=0.9$ is believed to be the critical point at which the P-P bond is fully formed.[10] This correspondence suggests that the intralayer dimensional variations in this family are more likely the result of P-P bond making and breaking than geometrical considerations. The electron-electron interaction is another effect correlated with the anomalous change in *T*-*T* bond length. As shown in Fig. 12, the increase of $\chi_{T=0}$ for $Ca(Fe_{1-x}Co_x)_2P_2$ is accompanying the anomalous *T*-*T* bond length variation. Further band-structure calculations are needed to investigate this interesting relationship.

The crystal and band structure are consistent with the magnetic properties of the $Ca(Fe_{1-x}Co_x)_2P_2$ and $Ca(Ni_{1-x}Co_x)_2P_2$ series. Although Fe and Ni are not simple magnetic "impurities" in $CaCo_2P_2$, Ni doping clearly introduces more complicated and localized magnetic behaviors. Similar Ni-induced localization was also observed in the isostructural $Tl(Co_{1-x}Ni_x)_2Se_2$ system.[26] Two factors can explain the more localized character for Ni doping: one is that the 3*d* band for Ni is narrower than Fe and the other is that the Ni-P bond is weaker than the Fe-P bond.[17] The weaker Ni-P bond likely introduces a more localized *d*-electron behavior. The *A*-type AFM ordering in $CaCo_2P_2$ is due to its relatively strong, intralayer FM interactions and relatively weak, interlayer AFM interactions. Following the P-P bond length variation, the magnetic interaction between the layers is expected to be stronger for Ni-rich members than for the Fe-rich members of this family. Therefore, with increased Ni doping, $Ca(Ni_{1-x}Co_x)_2P_2$ might have stronger interlayer AFM coupling, which suppresses θ_{CW}.

With few exceptions, the iron phosphides always show much lower T_c than iron arsenides.[27,28] The 122 iron phos-

phides do not show any superconducting while the 122 iron arsenides show that T_c is as high as 38 K in $Ba_{1-x}K_xFe_2As_2$. One explanation is that the iron phosphides have much larger P-Fe-P bond angles than the ideal tetrahedral angle of 109.47°. In iron arsenides the highest T_c is found for the ideal tetrahedron.[28] Our study shows that the P-*T*-P bond angle is nowhere near 109.47° for any Fe-Co or Ni 122 phosphides. de Haas-van Alphen measurements show that the 122 iron phosphides lack Fermi surface nesting compared to the analogous arsenides,[11] which may be due to the tetrahedron distortion for the phosphides. The *A*-type AFM ordering in $CaCo_2P_2$ also indicates that the magnetic interaction in the T_2P_2 layers in the phosphides is FM while in the parent compounds of iron arsenides the magnetic ordering is more frustrated, stripelike AFM. The frustrated AFM interaction in iron arsenides is believed to induce the structural distortion[29] and maybe the SC ground state, and this would not occur in the phosphides.

In conclusion, our experimental results reveal anomalous, non-Vegard's law *a*-axis variation in $Ca(Fe_{1-x}Co_x)_2P_2$. This anomaly indicates an underlying intralayer, electronic-structure change correlated with a monotonically decreasing interlayer P-P bond length upon electron doping. Both $Ca(Fe_{1-x}Co_x)_2P_2$ and $Ca(Ni_{1-x}Co_x)_2P_2$ evolve from a Pauli paramagnetic ($CaFe_2P_2$ and $CaNi_2P_2$) to antiferromagnetic ($CaCo_2P_2$) ground state with Co doping, through variation in the band structures. However, $Ca(Ni_{1-x}Co_x)_2P_2$ shows a more localized-electron behavior that results in more complicated magnetic phase transitions. The most significant effect of changing electron count on going from $CaFe_2P_2$ to $CaCo_2P_2$ to $CaNi_2P_2$ is to change the strength of the interlayer P-P bond; this unique change in structure, rather than simple rigid-bandlike *d*-orbital filling, must be driving the differences on observed physical properties.

ACKNOWLEDGMENT

The work at Princeton was supported by the U.S. Department of Energy, Division of Basic Energy Sciences under Grant No. DE-FG02-98ER45706.

[1] Y. Kamihara, T. Watanabe, M. Hirano, and H. Hosono, J. Am. Chem. Soc. **130**, 3296 (2008).
[2] H. Takahashi, K. Igawa, K. Arii, Y. Kamihara, M. Hirano, and H. Hosono, Nature (London) **453**, 376 (2008).
[3] M. Rotter, M. Tegel, and D. Johrendt, Phys. Rev. Lett. **101**, 107006 (2008).
[4] A. Kreyssig *et al.*, Phys. Rev. B **78**, 184517 (2008).
[5] P. Canfield, S. Bud'ko, N. Ni, A. Kreyssig, A. Goldman, R. McQueeney, M. Torikachvili, D. Argyriou, G. Luke, and W. Yu, Physica C **469**, 404 (2009).
[6] S. A. J. Kimber, A. Kreyssig, Y. Zhang, H. O. Jeschke, R. Valenti, F. Yokaichiya, E. Colombier, J. Yan, T. C. Hansen, T. Chatterji, R. J. McQueeney, P. C. Canfield, A. I. Goldman, and D. N. Argyriou, Nature Mater. **8**, 471 (2009).
[7] R. Hoffmann and C. Zheng, J. Phys. Chem. **89**, 4175 (1985).
[8] M. Reehuis, W. Jeitschko, G. Kotzyba, B. Zimmer, and X. Hu, J. Alloys Compd. **266**, 54 (1998).
[9] D. Johrendt, C. Felser, O. Jepsen, O. K. Andersen, A. Mewis, and J. Rouxel, J. Solid State Chem. **130**, 254 (1997).
[10] S. Jia, A. J. Williams, P. W. Stephens, and R. J. Cava, Phys. Rev. B **80**, 165107 (2009).
[11] J. G. Analytis, C. M. J. Andrew, A. I. Coldea, A. McCollam, J. H. Chu, R. D. McDonald, I. R. Fisher, and A. Carrington, Phys. Rev. Lett. **103**, 076401 (2009).
[12] A. I. Coldea, C. M. J. Andrew, J. G. Analytis, R. D. McDonald, A. F. Bangura, J.-H. Chu, I. R. Fisher, and A. Carrington, Phys. Rev. Lett. **103**, 026404 (2009).
[13] F. Ronning, E. D. Bauer, T. Park, S.-H. Baek, H. Sakai, and J. D. Thompson, Phys. Rev. B **79**, 134507 (2009).
[14] T. Mine, H. Yanagi, T. Kamiya, Y. Kamihara, M. Hirano, and H. Hosono, Solid State Commun. **147**, 111 (2008).
[15] W. Jeitschko and M. Reehuis, J. Phys. Chem. Solids **48**, 667 (1987).
[16] M. Reehuis and W. Jeitschko, J. Phys. Chem. Solids **51**, 961 (1990).
[17] E. Gustenau, P. Herzig, and A. Neckel, J. Solid State Chem. **129**, 147 (1997).
[18] I. B. Shameem Banu, M. Rajagopalan, M. Yousuf, and P. Shenbagaraman, J. Alloys Compd. **288**, 88 (1999).
[19] T. M. McQueen, M. Regulacio, A. J. Williams, Q. Huang, J. W. Lynn, Y. S. Hor, D. V. West, M. A. Green, and R. J. Cava, Phys. Rev. B **78**, 024521 (2008).
[20] B. H. Toby, J. Appl. Crystallogr. **34**, 210 (2001).
[21] A. C. Larson and R. B. V. Dreele, Los Alamos National Laboratory Report No. LAUR86, 2000 (unpublished).
[22] K. Schubert, *Kristallstrukturen zweikomponentiger Phasen* (Springer-Verlag, Berlin, Göttingen, 1964).
[23] J. A. Mydosh, *Spin Glass: An Experimental Introduction* (Taylor & Francis, London, 1993).
[24] V. Keimes, A. Hellmann, D. Johrendt, A. Mewis, and T. Woike, Z. Anorg. Allg. Chem. **624**, 830 (1998).
[25] E. Gustenau, P. Herzig, and A. Neckel, J. Alloys Compd. **262-263**, 516 (1997).
[26] A. R. Newmark, G. Huan, M. Greenblatt, and M. Croft, Solid State Commun. **71**, 1025 (1989).
[27] H. Ogino, Y. Matsumura, Y. Katsura, K. Ushiyama, S. Horii, K. Kishio, and J.-i. Shimoyama, Supercond. Sci. Technol. **22**, 075008 (2009).
[28] D. Johnston, arXiv:1005.4392 (unpublished).
[29] T. Yildirim, Phys. Rev. Lett. **101**, 057010 (2008).